# An Activation Gating Switch in Kv1.2 Is Localized to a Threonine Residue in the S2-S3 Linker

Saman Rezazadeh,* Harley T. Kurata,* Thomas W. Claydon,* Steven J. Kehl,† and David Fedida*
*Department of Anesthesiology, Pharmacology and Therapeutics, and †Department of Cellular and Physiological Sciences, University of British Columbia, Vancouver, British Columbia V6T 1Z3, Canada

ABSTRACT The activation properties of Kv1.2 channels are highly variable, with reported half-activation ($V_{½}$) values ranging from ~−40 mV to ~+30 mV. Here we show that this arises because Kv1.2 channels occupy two distinct gating modes ("fast" and "slow"). "Slow" gating ($\tau_{act} = 90 \pm 6$ ms at +35 mV) was associated with a $V_{½}$ of activation of +16.6 ± 1.1 mV, whereas "fast" gating ($\tau_{act} = 4.5 \pm 1.7$ ms at +35 mV) was associated with a $V_{½}$ of activation of −18.8 ± 2.3 mV. It was possible to switch between gating modes by applying a prepulse, which suggested that channels activate to a single open state along separate "fast" and "slow" activation pathways. Using chimeras and point mutants between Kv1.2 and Kv1.5 channels, we determined that introduction of a positive charge at or around threonine 252 in the S2-S3 linker of Kv1.2 abolished "slow" activation gating. Furthermore, dialysis of the cytoplasm or excision of cell-attached patches from cells expressing Kv1.2 channels switched gating from "slow" to "fast", suggesting involvement of cytoplasmic regulators. Collectively, these results demonstrate two modes of activation gating in Kv1.2 and specific residues in the S2-S3 linker that act as a switch between these modes.

## INTRODUCTION

Much of the machinery associated with voltage-gated potassium (Kv) channel activation is localized to a voltage-sensing domain (VSD) that comprises the transmembrane helices S1-S4, and includes a series of regularly spaced basic (Arg, Lys) residues in the S4 helix, together with acidic (Asp, Glu) residues in S2 and S3 helices (1–7). Considerable effort has been devoted to understanding the structural rearrangements during voltage gating, together with the conformational changes of the pore-forming domain that gate the permeation pathway (8–10). The detailed movements remain controversial (11–14), but it is well understood that membrane depolarization exerts forces on charged residues within the VSD, resulting in conformational changes that are coupled to the opening of a specialized ion-conducting pore formed by the S5 and S6 transmembrane helices (6,12,15). Much of the dynamic information that defines our understanding of Kv channel activation comes from the *Drosophila Shaker* channel, and so specific mechanisms that regulate the individual activation properties of mammalian Kv channels remain incompletely understood.

Although interactions between charged residues within the VSD (i.e., between basic residues in S4 and acidic residues in S2 and S3) are critical for normal activation gating (1,4), a number of studies demonstrate that other regions of the channel, especially the cytoplasmic N- and C- termini, can significantly modulate the time course and voltage dependence of activation. Deletion of either the N- or C-terminus of many channels, including Kv1.1, Kv1.2, Kv1.5, Kv2.1, and hERG, can substantially shift the voltage dependence of activation (16–24). In addition, the MTSET modification rate of thiol groups in the T1-T1 intersubunit interface of Kv4 channels is state dependent, which suggests significant conformational changes take place outside the VSD and the pore domain during channel gating (25).

Detailed studies of individual transmembrane domains of Kv channels have also identified regions other than those involved in interactions between the basic and acidic residues in S2, S3, and S4 that affect activation gating. For example, substitution of three noncharged amino acids from the *Shaw* channel S4 into *Shaker* channels (the ILT mutation) results in a dissociation of S4 movement from the concerted step in channel opening (26). In addition, exchange of the cytoplasmic half of S5 between Kv2.1 and Kv3.1 confers activation and deactivation properties similar to those of the donor channel without altering the voltage dependence of gating charge movements (27). Finally, a swap of S2 or S3 of Kv2.1 with that of Kv1.2 profoundly alters the activation time course (28).

In addition to these intrinsic structural influences on activation gating, the activation properties of Kv channels can also be modulated through protein-protein interactions or posttranslational modifications including phosphorylation and glycosylation. For example, it is well documented that the interaction of $\beta$-subunits with Kv channels results in modification of their activation and inactivation kinetics (29–32). In addition, coexpression of the $\beta$-subunit with $BK_{Ca}$ channels increases the sensitivity of activation to voltage and calcium without affecting single-channel conductance or ionic selectivity (33). Phosphorylation of squid giant axon $K^+$

*Submitted June 25, 2007, and accepted for publication July 27, 2007.*

Address reprint requests to Dr. David Fedida, Room 2.301, Life Sciences Centre, University of British Columbia, 2350 Health Sciences Mall, Vancouver, British Columbia V6T 1Z3, Canada. Tel.: 604-822-5806; Fax: 604-822-2316; E-mail: fedida@interchange.ubc.ca.

Harley T. Kurata's present address is Dept. of Cell Biology and Physiology, Washington University School of Medicine, St. Louis, Missouri 63110.

Editor: Richard W Aldrich.


0006-3495/07/12/4173/14 $2.00

doi: 10.1529/biophysj.107.116160

channels changes their activation kinetics, which is attributed to electrostatic interactions between the VSD and negatively charged phosphate groups (34,35). Similarly, dephosphorylation of Kv2.1 and Kv3.1 channels has been shown to result in a hyperpolarizing shift in the $V_{½}$ of activation (36–38). Finally, glycosylation of the S1-S2 linker of Kv1.1 and Kv1.2 channels results in a depolarizing shift in the $V_{½}$ of activation, an effect that is thought to be partly caused by the charge-screening effect of sialic acids (39–42).

Kv1.2, for which the atomic structure is known (43), is a Kv channel that shows quite variable activation kinetics. Most reports describe fast activation ($\tau < 10$ ms at +40 mV) with a $V_{½}$ of activation ranging from −15 mV to −43 mV (23,28,44,45). However, Grissmer et al. (46) briefly mentioned that Kv1.2 channels have a $V_{½}$ of activation of +27 mV and much slower activation gating ($\tau \approx 25$ ms at +40 mV), which becomes faster on repetitive pulsing. Here, we have extended these observations to show that Kv1.2 channels heterologously expressed in a number of different mammalian cell types can have two quite distinct activation phenotypes. ''Slow'' activation gating of Kv1.2 occurs during pulses applied after a rest interval and is associated with a depolarized $V_{½}$ of activation. Using a twin-pulse protocol, we show that activation gating can be switched into a ''fast'' mode and that this is associated with a large hyperpolarizing shift in the voltage dependence of activation gating. We demonstrate that this switch of gating is mediated at or around a single threonine residue, T-252, in the S2-S3 linker that is uniquely present in Kv1.2 among the Kv channels and that it can be modified by the presence or dialysis of cytoplasmic constituents. Furthermore, transfer of the S2-S3 linker from Kv1.2 to Kv1.5 channels introduced the heterogeneous activation properties of Kv1.2 channels in the otherwise consistently fast gating Kv1.5 channels. These data identify a novel mode of gating in Kv1.2 channels that may be regulated by interaction with a cytosolic component either at or associated with T-252 in the S2-S3 linker. This work has been presented in preliminary form as an abstract (47).

## MATERIALS AND METHODS

### Cell preparation and transfection

All experiments were carried out on transiently transfected mouse *ltk-* cells, HEK 293 cells, or CHO cells grown in minimal essential medium (MEM) with 10% fetal bovine serum, at 37°C in an air/5% $CO_2$ incubator. One day before transfection, cells were plated onto sterile glass coverslips in 35-mm petri dishes at 20–30% confluence. On the day of transfection, cells were washed once with MEM with 10% fetal bovine serum. To identify the transfected cells efficiently, channel DNA was cotransfected with a vector encoding green fluorescent protein (pGFP). Channel DNA was incubated with pGFP (1 $\mu$g of pGFP, 2 $\mu$g of channel DNA) and 3 $\mu$l of LipofectAMINE 2000 (Gibco-BRL, Burlington, Ontario, Canada) made up to 100 $\mu$l with serum-free OPTI-MEM (Gibco-BRL), then added to the dishes containing cells in 900 $\mu$l of MEM with 10% fetal bovine serum. Cells were allowed to grow overnight before recording.

### Solutions

Patch pipettes contained solution 1 (in mM): KCl, 135; EGTA, 5; HEPES, 10; adjusted to pH 7.2 with KOH. The bath solution contained solution 2 (in mM): NaCl, 135; KCl, 5; HEPES, 10; sodium acetate, 2.8; $MgCl_2$, 1; $CaCl_2$, 1; adjusted to pH 7.4 with NaOH. High external $K^+$ experiments were carried out using a bath containing solution 3 (in mM): KCl, 135; HEPES, 10; $MgCl_2$, 1; dextrose, 10; adjusted to pH 7.4 with KOH. For cell-attached and excised inside-out patch experiments, pipettes contained solution 2 while the bath contained solution 3. All chemicals were from Sigma Aldrich Chemical (Mississauga, Ontario, Canada).

### Electrophysiological procedures

Coverslips containing cells were removed from the incubator before experiments and placed in a superfusion chamber (volume 250 $\mu$l) containing the control bath solution at ambient temperature (22–23°C) and perfused with bathing solution throughout the experiments. Whole-cell, excised, and perforated patch current recording and data analysis were done using an Axopatch 200B clamp amplifier and pClamp 9 software (Axon Instruments, Foster City, CA). Patch electrodes were fabricated using thin-walled borosilicate glass (World Precision Instruments; Sarasota, FL). Electrodes had resistances of 1–3 MΩ when filled with control filling solution. Capacity compensation and 80% series resistance compensation were used in all whole-cell recordings. No leak subtraction was used when recording currents, and zero current levels are denoted by the dashed lines in the current panels. Data were sampled at 10–20 kHz and filtered at 5–10 kHz. For perforated patch experiments, 100 $\mu$g/ml of nystatin was added to the pipette solution (solution 1). After the gigaohm seal between tip and cell membrane had formed, negative pressure was released to await gradual opening of nystatin-induced pores. Recordings were made only after the access resistance was <20 MΩ. Membrane potentials have not been corrected for small liquid junction potentials between bath and pipette solutions.

### Molecular biology and channel expression

The mammalian expression vector pcDNA3 was used for expression of all channel constructs used in this study. Kv1.2 constructs were kind gifts of Dr. D. Minor (UCSF) and Dr. B. Tempel (University of Washington). All primers used were synthesized by Sigma Genosys (Oakville, Ontario, Canada). All constructs were sequenced to check for errors and to ensure the correct reading frame (NAPS Unit, University of British Columbia, Vancouver, British Columbia, Canada).

### Kv1.5/Kv1.2 Chimeras

Chimeras were constructed by PCR amplification of the desired segment of Kv1.2, introducing restriction sites to allow subcloning into the Kv1.5 cDNA. With the exception of the Kv1.2/Kv1.5C chimera, an *Eco*RI restriction site was introduced at the C-terminal end of the fragment, and either a *Bsp*EI (for Kv1.5N/Kv1.2), *PmlI* (for Kv1.5S1S2L/Kv1.2), *Cla*I (for Kv1.5S2S3L/Kv1.2), or *Stu*I (for Kv1.5S4S5L/Kv1.2) was introduced at the N-terminal end of the fragment. For construction of the Kv1.2/Kv1.5C chimera, the Kv1.5 C-terminus was amplified by PCR, introducing 5′ and 3′ *Hpa*I restriction sites, and subcloned into the Kv1.2 cDNA as an *Hpa*I-*Hpa*I fragment. Point mutations in Kv1.2 and Kv1.5 were generated using the Stratagene Quikchange kit (Stratagene, La Jolla, CA).

### Data analysis and modeling

The *g-V* curves throughout the text were derived using the normalized chord conductances, which were calculated by dividing the maximum current

elicited during a depolarizing step by the driving force derived from the calculated $K^+$ equilibrium potential. The *g-V* curves were fitted with a single Boltzmann function of the form: $y = 1/(1 + \exp[V_{½} - V]/k)$ where $y$ is the conductance normalized with respect to the maximal conductance, $V_{½}$ is the half-activation potential, $V$ is the test voltage, and $k$ is the slope factor. Data throughout the text and figures are shown as mean ± SE. Statistical significance was determined throughout using Student's *t*-test with $p$ values of $<0.05$ taken to be significant.

Macroscopic Kv1.2 currents were simulated using a scientific graphing package (IGOR 5, Wavemetrics, Lake Oswego, OR) in which state occupancies as a function of time and voltage were derived from the spectral expansion of the *Q*-matrix (48) generated from the state diagram (see Fig. 9 *A*). For the calculation of currents, the open-channel *I-V* relationship was assumed to be ohmic. The rate constant for transition $x$ at a given voltage ($k_x(V)$) was calculated from the equation: $k_x(V) = k_x(0\text{ mV})\exp(z_xFV/RT)$ where F, R, and T have their usual meanings, $k_x(0\text{ mV})$ is the rate constant at 0 mV, and $z_x$ is the equivalent charge moved between state $x$ and the transition state. In the upper row the parameters were: $k_{f,f}(0\text{ mV}) = 420\text{ s}^{-1}$, $k_{b,f}(0\text{ mV}) = 373\text{ s}^{-1}$, $z_{kf,f} = 0.25$, $z_{kb,f} = -0.8$, $k_{co,f} = 8000\text{ s}^{-1}$, and $k_{oc,f} = 100\text{ s}^{-1}$. This approach and the values used to simulate ''fast'' activation are similar to those used for *ShakerIR* currents (26) and suggested to be appropriate for Kv1.2 (45). To replicate ''slow'' activation, a parallel activation pathway was added (*lower row*) with the same kinetic behavior as the upper fast pathway except that the concerted transitions ($C_{10}\rightarrow O_5$ and $C_{10}\leftarrow O_5$) were slowed. Rate constants ($k_{fs}$, $k_{sf}$) for vertical transitions between the ''fast'' and ''slow'' activation pathways were assumed, again for simplicity, to be voltage-independent and were assigned values to approximate the time-dependence for the relaxation from the ''fast'' activation pathway to the ''slow'' activation pathway in a two-pulse voltage protocol (see below). The horizontal kinetic parameters were the same as the corresponding values in the upper row, except: 1), $k_{f,s}(0\text{ mV})$ was $140\text{ s}^{-1}$; 2), $k_{co,s}$ was $40\text{ s}^{-1}$; and, 3), $k_{oc,s}$ was $1\text{ s}^{-1}$. The variables $g$ and $d$ were required to conserve microscopic reversibility. With $k_{fs} = 0.022$ and $k_{sf} = 0.0088$, as was the case for all traces except for the fast-activating currents in Fig. 9 *B*, then $g = (k_{co,f}k_{oc,s}k_{sf}/k_{oc,f}k_{co,s}k_{fs})^{0.5} = 0.89442$; and $d = (k_{f,s}k_{b,f}/k_{f,f}k_{b,s})^{0.5}$, which simplifies to $d = (k_{f,s}/k_{f,f})^{0.5}$ because the rate constants $k_{b,f}(V)$ and $k_{b,s}(V)$ are identical and because $k_{f,f}$ and $k_{f,s}$ have the same voltage dependence, $d$ has a fixed value of 0.57735. To reduce the number of fitting parameters, it was assumed that the concerted opening ($C_4\rightarrow O_5$, $C_{10}\rightarrow O_5$) or concerted closing ($C_4\leftarrow O_5$, $C_{10}\leftarrow O_5$) transitions were voltage independent, but making these transitions voltage dependent is not expected to substantially change the outcome.

## RESULTS

### Heterogeneous activation properties of Kv1.2 expressed in mammalian cell lines

Initial characterization of Kv1.2 using whole-cell patch clamp recordings from mouse *ltk-* cells revealed a considerable variation in both the time course and $V_{½}$ of channel activation. Chord conductance was measured from currents during 400-ms activating voltage steps, and individual conductance-voltage relationships from 70 cells are plotted in Fig. 1 *A* to illustrate that activation relationships fell broadly into two groups, with isochronal $V_{½}$ estimates ranging between ~−35 mV and ~+35 mV. It appears that Kv1.2 shows two very distinct activation curve voltage dependencies, with one population of cells showing isochronal activation $V_{½}$s $< -10$ mV and a second population of cells with isochronal activation $V_{½}$s more positive than +10 mV.

We also observed considerable differences in the speed of channel activation (Fig. 1, *B–D*). A proportion (27%) of cells expressing Kv1.2 exhibited a rapid activation time course, much of which could be fit with a single exponential ($\tau$ = 4.5 ± 1.7 ms at +35 mV), reminiscent of *Shaker* and related mammalian Kv1 channels (Fig. 1 *B*). However, a larger proportion of cells exhibited much slower kinetics of activation (48%; $\tau$ = 90 ± 6 ms at +35 mV, Fig. 1 *C*) or biphasic activation kinetics with fast and slow components in varying proportions (25%) (Fig. 1 *D*). As a first analysis we grouped individual 400-ms activation curves (Fig. 1 *A*) based on the activation kinetics into ''fast'' cells (*black lines*), ''slow'' cells (*red lines*), and ''mixed'' cells (*dashed black lines*). Mean activation curves for cells falling into each group (Fig. 1 *E*) revealed that cells exhibiting ''fast'' kinetics also exhibited current activation at negative voltages ($V_{½}$ = −18.8 ± 2.3 mV, $n = 19$). Cells that exhibited ''slow'' or mixed activation kinetics had $V_{½}$s of 16.6 ± 1.1 mV ($n = 33$) and 14.5 ± 1.6 mV ($n = 18$), respectively ($p > 0.05$). To illustrate the dramatic difference between the ''slow'' and ''fast'' gating phenotypes that we observed for Kv1.2, currents at +55 (from a slow cell) and +15 mV (from a fast cell), where $P_o$ was maximal, have been normalized to peak current and overlaid (Fig. 1 *F*). Critically, the differences in activation kinetics do not appear to be simply results of the different $V_{½}$s in cells exhibiting these various phenotypes. Single exponential fits to the activation time course to estimate activation kinetics demonstrated that, even with strong depolarizations, the activation kinetics in ''slow'' cells remained considerably slower than those observed in ''fast'' cells even at the most positive potentials studied (Fig. 1 *G*). Overall, the proportions of cells exhibiting the various phenotypes were 27% (fast) and 73% (slow or mixed), respectively, in *ltk-* cells, and a similar ratio was observed for Kv1.2 channels expressed in other mammalian cell lines including CHO and HEK 293 cells (Fig. 1 *H*). Because *ltk-* cells showed little or no endogenous currents, and because constructs expressed well in these cells, this cell line was used for the remaining experiments in the study.

Previous experience with recordings from other Kv channels in mammalian cell lines has accustomed us to high reproducibility of activation kinetics among individual cells. We ruled out the possibility of contamination of the DNA used for transfections by repeatedly selecting and sequencing clones from individual *Escherichia coli* transformants. In addition, we noticed that although this dramatic variability has not been reported in any individual study of Kv1.2, there are considerable discrepancies of reported activation $V_{½}$s, ranging from −43 mV (44), −24.6 mV (23), and −17.9 mV (28), up to +27 mV (46) and +22 mV (49).

### Prepulse potentiation of Kv1.2 activation

One very early report examining the pharmacology of Kv1.2 had suggested a use-dependent activation process, with

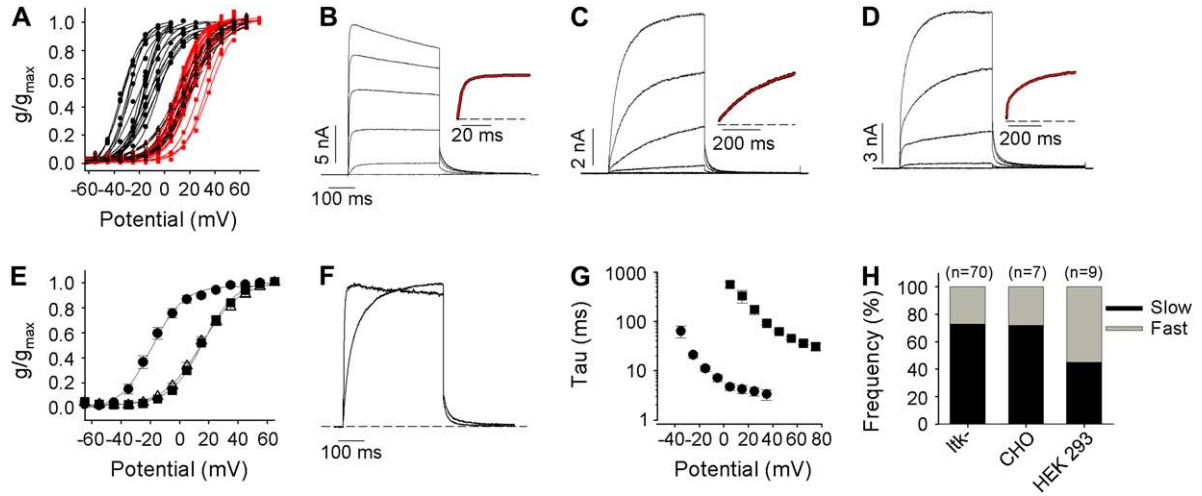


FIGURE 1 Bimodal gating of Kv1.2 expressed in mammalian cell systems. (*A*) Isochronal *g-V* relationships from seventy *ltk-* cells transiently expressing Kv1.2. Normalized maximum chord conductance during 400-ms pulses was determined for each membrane potential, and the data from individual cells were fitted with a Boltzmann function. (*B–D*) Examples of current-voltage data in *A*. Currents were elicited by depolarizing steps from −65 to +55 mV in 20-mV increments. The gating kinetics of Kv1.2 showed three clear phenotypes: a group that expressed very fast activation kinetics, plotted as (●) in *A* and shown in *B*; a group that exhibited dramatically slower opening, plotted as (*red* ■) in *A* and shown in *C*, both of which were fitted with single exponential functions (*insets* illustrate the fitted currents recorded at +15 mV); and an intermediate phenotype, plotted as Δ in *A* and shown in *D* with a mixture of ''fast'' and ''slow'' activating channels, whose activation time course was fitted with a double exponential function. Solid black, solid red, and broken black lines in *A* represent Boltzmann fits to data from fast, slow, and mixed activating phenotypes, respectively. (*E*) The mean isochronal activation $V_{½}$ was −18.8 ± 2.3 mV ($n = 19$, $k = 9.1 \pm 0.5$ mV) for ''fast'' activating channels (●), 16.6 ± 1.1 mV (■) for slowly activating channels ($n = 33$, $k = 10.1 \pm 0.3$ mV), and 14.5 ± 1.6 mV ($n = 18$, $k = 12.5 \pm 1.5$ mV) for mixed channels (Δ). (*F*) Examples of normalized currents at +15 and +55 mV ($P_o \sim 1.0$) for ''fast'' and ''slow'' activating phenotypes. (*G*) Monoexponential activation time constants for ''fast'' (●) and ''slow'' (■) activating channels. (*H*) Modal gating was observed for Kv1.2 in *ltk-*, CHO, and HEK 293 cells.

acceleration of activation kinetics and enhancement of Kv1.2 currents during trains of repetitive depolarizations (46). We investigated this phenomenon further with a twin-pulse protocol (Fig. 2 *A*). Cells expressing Kv1.2 were pulsed to voltages between −50 and +40 mV (P1, 1.5 s), repolarized (200 ms) to −80 mV, and finally pulsed to +20 mV (P2, 1.5 s). In cells exhibiting the ''slow'' activation phenotype, the kinetics of activation in the P2 pulse depended dramatically on the voltage during the P1 pulse (Fig. 2 *A*). If the voltage during the P1 pulse did not lead to significant opening of channels (e.g., <−20 mV), the activation kinetics during P2 were very slow. In contrast, when the P1 voltage led to significant channel opening (e.g., +40 mV), activation kinetics during P2 became very fast. This ''prepulse potentiation'' resulted in significantly accelerated activation kinetics and greater current amplitude at the end of the P2 pulse (*shaded trace*, Fig. 2 *B*) than when the channels activated slowly (*solid trace*, Fig. 2 *B*). Application of prepulse to ''fast'' gating channels did not result in potentiation of ionic currents (Fig. 2 *C*).

Channel activation before and after prepulse conditioning had different voltage dependencies (Fig. 2, *D* and *E*). Cells exhibiting the ''slow'' gating phenotype were pulsed to voltages between −65 mV and +35 mV for 2 s and then repolarized to −40 mV to allow calculation of an activation curve for slowly activating channels (Fig. 2 *E*, *negative prepulse*). The $V_{½}$ of activation of slowly activating channels calculated from 2-s depolarizing steps in Fig. 2 *E* is somewhat hyperpolarized compared with the relation in Fig. 1 *E*, obtained from 400-ms pulses, and this is the result of allowing channel activation to reach a steady state. In the same cells, the effect of prepulse potentiation was determined by including a 1-s prepulse to +40 mV before the activation protocol (Fig. 2 *D*). The prepulse accelerated channel activation and resulted in an ∼−30 mV hyperpolarizing shift in the $V_{½}$ of channel activation (Fig. 2 *E*, data, + *prepulse*). Such a prepulse-dependent gating shift in Kv channels is unexpected, and these data raise the possibility that activation of ''slow'' channels during the prepulse permits subsequent activation via a separate pathway that is more permissive to channel opening, presumably through the same pathway that the ''fast'' activation gating proceeds. Consistent with this, application of a prepulse to ''fast'' channels did not result in a shift in the $V_{½}$ of channel activation (Fig. 2 *F*).

## Voltage-dependent recovery of ''slow'' activation

It is possible that the acceleration of activation kinetics after a prepulse is simply the consequence of very slow deactivation after the first pulse or very slow backward transitions through one or more closed states on repolarization. To test whether a very slow initial step in channel closure was responsible for the acceleration in activation kinetics, tail

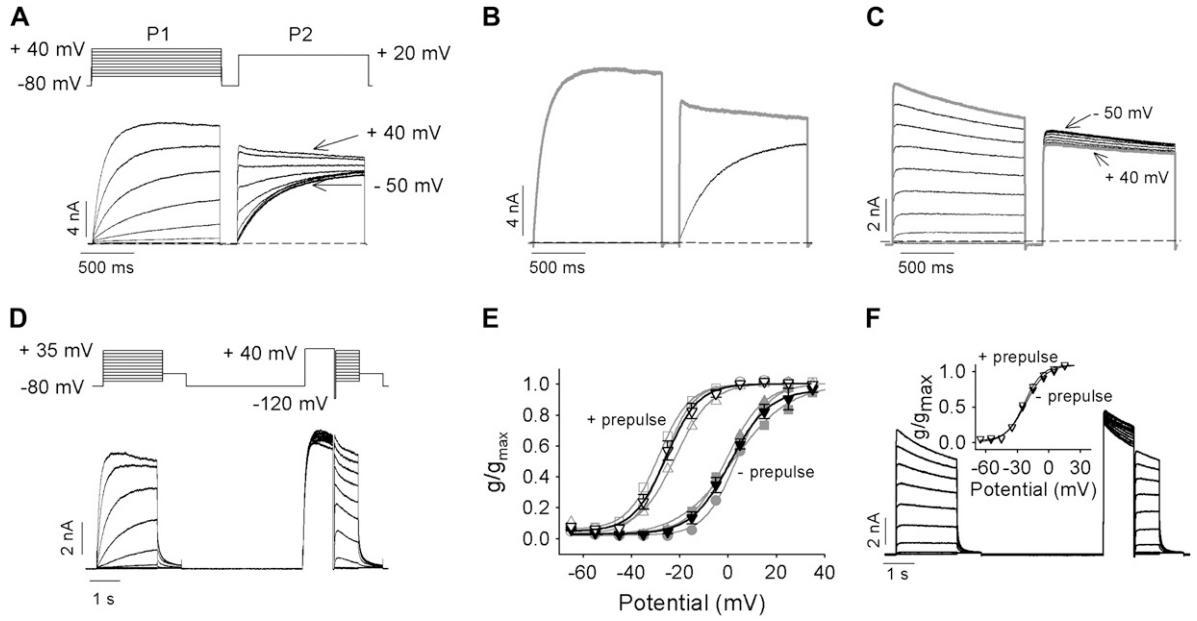


FIGURE 2 Twin pulses convert ''slow'' to ''fast'' activation in Kv1.2. (*A*) Twin-pulse voltage protocol is shown above, currents below recorded between −50 mV and +40 mV in 10-mV increments for 1.5 s, repolarized to −80 mV for 200 ms, and then depolarized to +20 mV for 1.5 s from a cell exhibiting the ''slow'' gating mode. Labels on currents refer to the P1 pulse potential. (*B*) Example of currents from *A* at +20 mV with (*shaded trace*) and without (*black trace*) a prepulse to +40 mV. (*C*) Ionic currents recorded from a cell exhibiting the ''fast'' gating mode using the protocol shown in *A*. The shaded trace depicts the current at +20 mV with a +40 mV prepulse. (*D* and *E*) Normalized *g-V* relations before and after a +40 mV prepulse from cells exhibiting the ''slow'' gating mode. Original, continuous data shown in *D*, for pulses between −65 and +35 mV in 10-mV steps obtained using the voltage protocol above. After the first set of voltage steps, the cell was repolarized to −80 mV for 4 s and then given a 1-s prepulse to +40 mV before a 50-ms repolarization to −120 mV and finally the second set of voltage steps. (*E*) Maximum normalized conductance from three cells obtained for the first (*solid symbols*) and the second set of steps (*open symbols*) plotted against membrane potential and fitted with a Boltzmann function. A switch in channel activation gating from ''slow'' to fast between the first and second set of clamp pulses shifted the mean activation $V_{½}$ from 1.8 ± 1.5 mV to −25.7 ± 2.0 mV ($n = 3$). Mean relationships are plotted as black lines and symbols. (*F*) The effect of a +40 mV prepulse on the *g-V* relations in cells exhibiting the ''fast'' gating mode. Ionic traces were recorded using the protocol shown in *D*. The inset illustrates the average maximum normalized conductance from three cells obtained from the first (*solid symbols*) and the second set of steps (*open symbols*) plotted as a function of membrane potential and fitted with a single Boltzmann function. The $V_{½}$ values were −22.1 ± 0.8 mV and −22.3 ± 1.0 mV for without and with prepulse, respectively.

currents in the presence of 135 mM extracellular $K^+$ were examined (Fig. 3 *A*). Large inward tail currents were observed during repolarization to −80 mV that decayed rapidly and completely within the P1-P2 interval duration. The tails could be fit with single exponential functions and had a mean time constant of decay of 12.9 ± 3.2 ms at −80 mV ($n = 5$). This suggested that failure of channel closure was not responsible for the rapid activation of current during the second step of a two-pulse protocol (Figs. 2 *B* and 3 *A*). In addition, the slow activation kinetics of Kv1.2 were relatively insensitive to changes in holding potential, as it was observed that activation kinetics changed very little as the holding potential was altered between −40 mV and −120 mV (Fig. 3 *B*).

It was noted in Fig. 2 *B*, that when the interval between P1 and P2 was brief, the P2 activation was very rapid. In Fig. 3, *C–F*, this experiment was repeated at different interpulse potentials, and as the P1-P2 interval was prolonged at each interpulse potential, the time dependence of recovery of the slow component of channel activation could be seen. Clearly, the recovery of the slow component of channel activation was fastest when channels were held at voltages near the threshold of channel opening (e.g., −40 mV) during the P1-P2 interval (Fig. 3 *C*), and recovery was much slower at extremely hyperpolarized voltages (e.g., −120 mV, Fig. 3 *E*). Fits to the time courses of recovery gave mean time constants of 1.45 s, 2.4 s, and 2.75 s at interpulse potentials of −40 mV, −80 mV, and −120 mV, respectively. This observation is the opposite of what would be expected if prepulse potentiation were the result of incomplete deactivation of channels. Collectively, these data demonstrate that the prepulse potentiation observed in Kv1.2 was not the result of incomplete closure during the interpulse interval and that it could instead arise from entry of channels into an alternative activation pathway more permissive to channel opening.

## Molecular determinants of prepulse potentiation

Data presented thus far have demonstrated that the activation kinetics of Kv1.2 can show two distinct phenotypes. One population of cells exhibited ''fast'' behavior, characterized by rapid activation kinetics insensitive to prepulse potentiation, whereas a second group of cells exhibited ''slow''

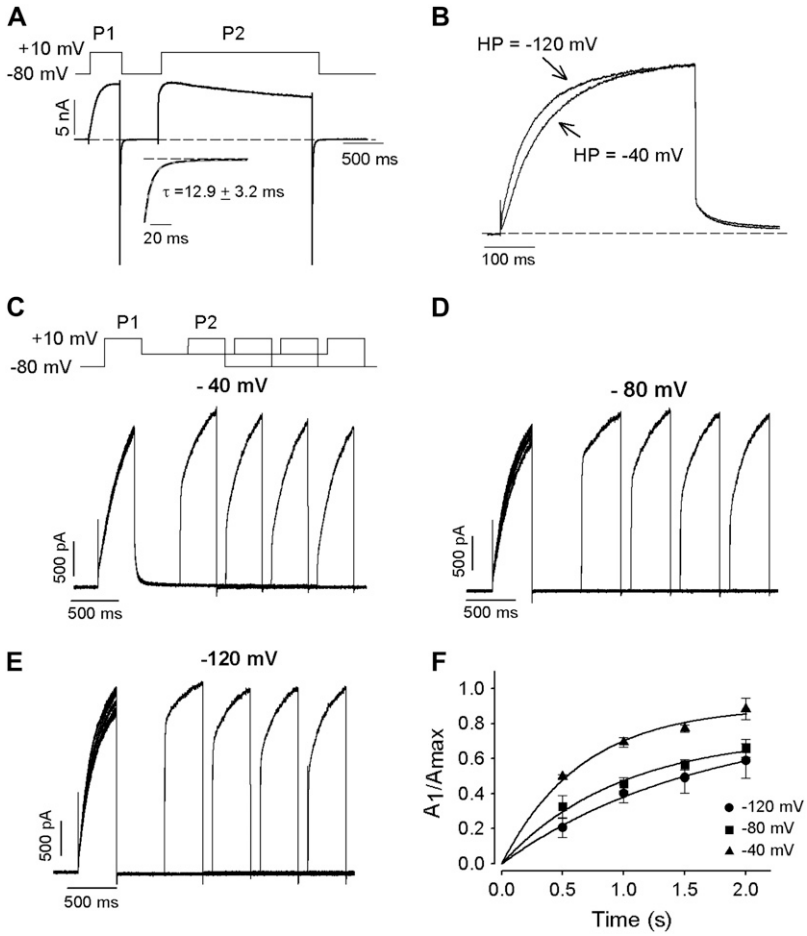


FIGURE 3 Holding potential has little effect on slow activation kinetics of Kv1.2 and voltage-dependent recovery of slow activation in Kv1.2. (*A*) The rate of deactivation at −80 mV was assessed in symmetrical 135 mM $K^+$. The cell was pulsed to +10 mV to reveal slow activation and then repolarized to −80 mV. Complete deactivation of the tail current was seen before the second pulse to +10 mV revealed rapid current activation. The inset illustrates the fitted tail current at −80 mV. (*B*) The cell was held at either −120 mV or −40 mV for 1 min before application of a depolarizing pulse to +30 mV. Each trace was fitted to a first-order exponential function, and activation time constants were determined to be 92 ms and 72 ms for the −40 mV and −120 mV potentials, respectively. (*C–E*) Recovery of slow activation kinetics as a function of the interpulse holding potential, −40 mV (*C*), −80 mV (*D*), or −120 mV (*E*). Protocol is shown for −40 mV experiment. Activation of current traces was fit with a double exponential function, and the normalized amplitude of the slow component ($A_1/A_{max}$) was plotted against recovery time (*F*). Fits to the time course gave mean time constants of recovery of 1.45 s, 2.4 s, and 2.75 s at interpulse potentials of −40 mV, −80 mV, and −120 mV, respectively ($n = 4$).

behavior, characterized by extremely slow activation kinetics that could be accelerated by conditioning channels with a prepulse. To our knowledge, this heterogeneity of activation kinetics, if not unprecedented, is rare among the known Kv channels. Our previous studies of Kv1.5 and other Kv1 channels showed no hint of such regulation of channel activation, with extremely consistent kinetics and steady-state behavior observed between cells (50). Therefore, we adopted a chimeric strategy, and progressively substituted the Kv1.2 sequence with corresponding residues from Kv1.5, beginning from the N-terminus (Fig. 4 *A*). The purpose of this chimeric study was to isolate a segment of Kv1.5 that could abolish the unique ''slow'' activation gating phenotype characterized in Kv1.2 and hence abolish the cell-to-cell heterogeneity of Kv1.2 activation gating. To this end, the activation kinetics of the Kv1.2/Kv1.5 chimeras were characterized, with a particular focus on the proportion of cells exhibiting the ''slow'' versus ''fast'' activation phenotype.

Substitution of the Kv1.5 sequence comprising the cytoplasmic N-terminus, or up to the beginning of the S2 transmembrane segment, did not abolish ''slow'' activation in Kv1.2. In the Kv1.5N/Kv1.2 chimera, and the Kv1.5S1S2L/Kv1.2 chimera, the frequency of the ''slow'' gating phenotype was reduced relative to Wt Kv1.2 channels but was nevertheless clearly observed in one-third of cells (Fig. 4, *B* and *C*). Interestingly, further substitution of the Kv1.5 sequence comprising the S2 transmembrane segment and the cytoplasmic S2-S3 linker (Kv1.5S2S3L/Kv1.2 chimera, Fig. 4, *B* and *C*) completely abolished the ''slow'' gating behavior in the 23 cells examined. Consistent with this observation, chimeras with further substitution of Kv1.5 sequence up to the cytoplasmic side of the S5 transmembrane helix (Kv1.5S4S5L/Kv1.2, Fig. 4) exhibited none of the slowly activating currents that were observed in Wt Kv1.2. A chimera comprising the C-terminus of Kv1.2 substituted with Kv1.5 sequence clearly did not abolish the ''slow'' activation phenotype but rather increased its frequency (this mutation expressed very poorly, hence the low sample size).

The chimeric studies, and particularly the difference between the Kv1.5S1S2L/Kv1.2 and Kv1.5S2S3L/Kv1.2 chimeras, suggested an important role for the S2 transmembrane helix and/or the S2-S3 linker in the regulation of Kv1.2 gating. To confirm this, we transferred this region from Kv1.2 into Kv1.5 and assessed whether this was sufficient to convert the consistently fast gating of Kv1.5 channels into a

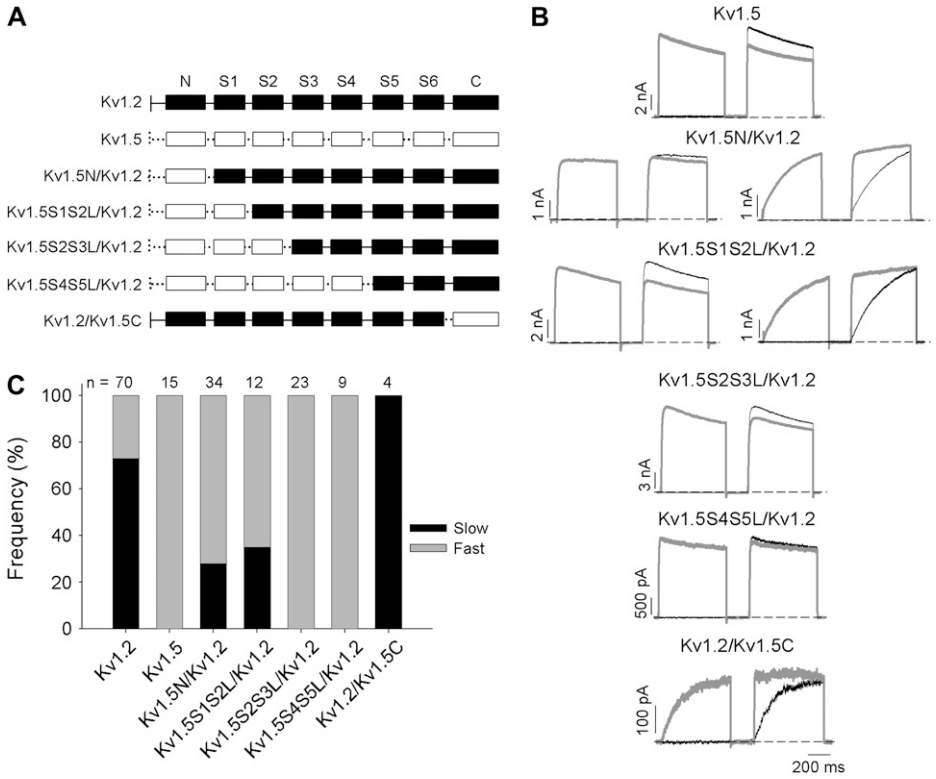


FIGURE 4 Chimeric study of Kv1.5 and Kv1.2 domains that regulate activation rate. (*A*) Schematic diagram of chimeras constructed. Kv1.2 domains are shown in solid boxes joined by continuous lines, whereas Kv1.5 domains are shown in open boxes joined by perforated lines. (*B*) The activation of each construct was assessed using the twin-pulse protocol (Fig. 2) with either a −50 mV or +40 mV step, followed by a +40 mV test potential in the second step. Data with the +40 mV prepulse are shown in gray. The interpulse potential was −100 mV for 200 ms. Where constructs showed both ''fast-'' and ''slow''-activating phenotypes, an example of each is shown. (*C*) The frequency of ''slow'' and ''fast'' activation for each construct is shown as the proportion of solid and shaded in the bar graph, respectively. The number of cells studied for each construct is shown above.

more heterogeneous phenotype (Fig. 5). It is clear that after transfer of the S2 transmembrane helix and S2-S3 linker from Kv1.2 to Kv1.5, activation properties could be divided into two groups. One group of cells exhibited ''fast'' activation kinetics with a hyperpolarized $V_{½}$ of activation (Fig. 5, *A* and *B*), whereas the other group exhibited ''slow'' activation kinetics that could be accelerated by prepulse potentiation and displayed a depolarized $V_{½}$ of activation. Together, these data demonstrate the importance of the S2 transmembrane helix and S2-S3 linker in the regulation of the activation properties of Kv1.2.

## A critical threonine in the S2-S3 linker of Kv1.2

Sequence alignment of the S2 and S2-S3 linker revealed six amino acid differences between Kv1.2 and Kv1.5 (Fig. 6 *A*, *asterisked residues*). Because of the chimera design, only five of these amino acids (Kv1.2 residues 230, 234, 237, 251, and 252) differed between the Kv1.5S1S2L/Kv1.2 and Kv1.5S2S3L/Kv1.2 chimeras (Fig. 6 *A*). These were individually replaced in Kv1.2 with the corresponding Kv1.5 residue and the activation kinetics of each point mutant characterized (Fig. 6 *B*), again paying particular attention to the relative frequency of ''fast'' versus ''slow'' activation gating (Fig. 6 *C*). Interestingly, in four of five point mutants, the ''slow'' gating phenotype was predominant. Although the proportion of cells expressing ''slow'' gating S234T channels was less than that observed for Wt Kv1.2 channels studied concurrently (Fig. 6 *C*), it was similar to the mean data from a large group of cells expressing Wt Kv1.2 channels (Fig. 1 *H*), suggesting that the S234T mutant displayed similar heterogeneous gating behavior to Wt Kv1.2 channels. The T252R mutation, however, which is predicted to lie within the cytoplasmic S2-S3 linker, completely abolished the ''slow'' gating phenotype in all 33 cells, which were tested over the course of many days (Fig. 6 *C*). To ensure that these data were not compromised by day-to-day variability of cell behavior, experiments with Wt Kv1.2 channels were generally performed in parallel, as shown by the Wt data bars in Fig. 6 *C* (11 of 12 showed slow gating). Apart from these functional data, sequence alignment with other Kv1 channels also suggests a unique and important role for T252 in Kv1.2. Among all other Kv1 channels, and nearly universally among Kv channels, the equivalent residue is basic, either arginine (R) or lysine (K) (Fig. 6 *A*).

To further examine the functional importance of T252 in Kv1.2, the effects of amino acid substitutions with various chemical properties were made at this site and the adjacent residues G249 to I254 (Fig. 7). As mentioned above, substitution with the basic amino acid arginine completely abolished the ''slow'' gating phenotype observed in Wt Kv1.2 channels (Fig. 6 *C*). Similarly, substitution with lysine or cysteine completely abolished the ''slow'' gating behavior of Kv1.2 (Fig. 7 *A*). With either substitution (T252C or T252K), ionic currents recorded over a wide range of

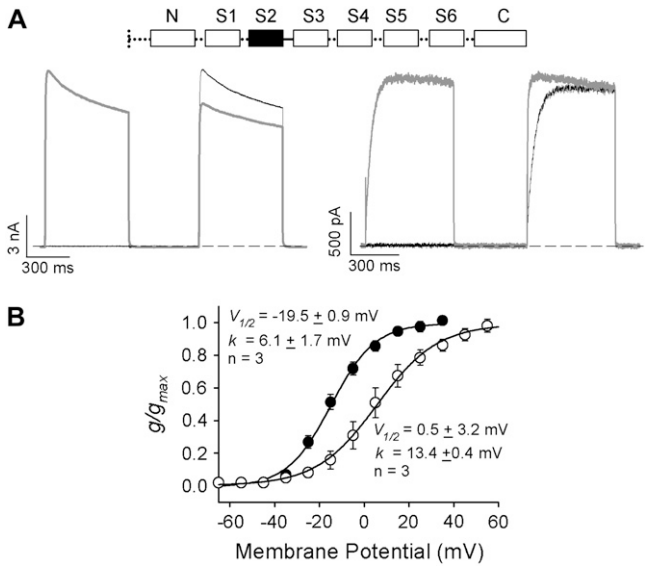


FIGURE 5 Transfer of the S2 helix and S2-S3 linker from Kv1.2 to Kv1.5 confers modal activation gating kinetics. (*A*) Representative ionic currents recorded from cells expressing chimeric channels with the S2 and S2-S3 linker of Kv1.5 substituted with that of Kv1.2 (*inset*, Kv1.2 domain is shown in *solid boxes*, and the linker by a *continuous line*, whereas Kv1.5 domains are shown in *open boxes* joined by *perforated lines*) during the twin-pulse protocol with either a −50 mV or a +40 mV step, followed by a +40 mV test potential in the second step. Data with the +40 mV prepulse are shown in gray. The interpulse potential was −100 mV for 500 ms. Transfer of the S2 helix and S2-S3 linker from Kv1.2 channels conferred variable gating kinetics to the normally invariant rapidly activating Kv1.5 channels. ''Slow'' gating kinetics that demonstrated prepulse potentiation were observed in 50% of cells. Typical examples of ''fast'' and ''slow'' gating in this channel are shown in panel *A*. (*B*) Isochronal *g-V* relationships from Kv1.5N/Kv1.2S1-S2S3L/Kv1.5 channels confirm the bimodal gating. The activation relationships fell into two groups with $V_{½}$ values ranging from −19.5 mV in the ''fast'' gating cells to +0.5 mV in the ''slow'' gating cells.

potentials activated rapidly (Fig. 7, *B* and *C*) and at negative potentials (Fig. 7 *E*). The twin-pulse protocol applied to these mutants revealed no prepulse potentiation (Fig. 7, *B*, *C*, and *insets*). Activation curves were reproducible between cells and did not display the heterogeneity recorded from Wt Kv1.2 (Figs. 1 *A* and 7 *E*). The mean $V_{½}$ of activation was −14 ± 1 mV ($n$ = 12) in T252C and −10.3 ± 1.0 mV ($n$ = 4) in T252K, and neither was significantly different from the $V_{½}$ of ''fast'' activating Wt Kv1.2. The T252D mutant (Fig. 7 *D*) exhibited ''slow'' gating behavior in 13 of 14 cells (93%) with a mean $V_{½}$ of activation of +9.8 ± 2.3 mV. This ''slow'' gating percentage was similar to that observed with Wt Kv1.2 (90%), recorded in parallel experiments (Fig. 7 *A*). Similar Wt-like heterogeneous gating was observed with T252A, T252E, T252M, and T252N (Fig. 7 *A*). On the other hand, substitution of arginine at position 250 or 251 for phenylalanine (F250R and F251R) was able to promote an exclusively ''fast'' activation gating in Kv1.2, as it had for T252R and T252K. This effect appeared highly localized because substitution with an arginine at 249 (G249R) or 253 (N253R) did not induce exclusively fast activation gating. These results point to a local effect of charged substitutions around T252 as a potent regulatory mechanism for the time and voltage dependence of activation gating in Kv1.2.

## Cytoplasmic constituents regulate Kv1.2 channel gating

In a number of cells expressing Wt Kv1.2, we observed a permanent switch from ''slow'' to ''fast'' activation gating kinetics over time (Fig. 8 *A*). This switch occurred gradually over a period of 90 s (Fig. 8 *A*, *left panel*), suggesting that dialysis of the cellular constituents could cause the switch of gating to occur. In support of this, prevention of dialysis, by using the perforated-patch-clamp configuration (Fig. 8 *B*), preserved the ''slow'' gating mode in all cells tested even during experiments that were 30 min in duration. Furthermore, excision of inside-out patches from the cytosolic environment (Fig. 8 *C*) rapidly switched all channels from the ''slow'' to the ''fast'' gating mode on formation of the excised patch. Taken together, these data suggest that Kv1.2 activation gating may be regulated by an unknown cytoplasmic element that can be removed from the channel after whole-cell dialysis or patch excision and is in sufficiently limited concentrations that its effect can be overcome at high levels of channel expression.

Many cytoplasmic mediators of $K^+$ channel function have been identified (51–53). To identify the cytosolic factor modifying Kv1.2 gating, we investigated the effects of key candidates on the ability of Kv1.2 channels to operate in the two modes of activation. Selective inhibition of a number of Ser/Thr kinases (PKC, PKA, PKG, CaMKII, and MLCK) by incubation or dialysis of cells expressing Kv1.2 channels with selective blockers (bisindolylmaleimide, H-89, PKG inhibitor, KN-93 and ML-7, respectively) or a broad range inhibitor (staurosporine) resulted in no measurable change in the frequency of the two activation gating modes (data not shown). Furthermore, cleavage of all the bound phosphate groups by dialysis of cells, through the patch pipette, with a very high concentration of alkaline phosphatase (100 U/ml; New England BioLabs, Ipswich, MA) resulted in no change in channel-activation properties (data not shown).

Other than phosphorylation, $K^+$ channel function is also known to be modulated by phospholipids, such as $PIP_2$, and cytoplasmic polyamines. However, addition of 10 $\mu$g/ml $PIP_2$ or 1 mM spermidine to the intracellular face of excised inside-out patches of membranes containing Wt Kv1.2 channels had no effect on the channel-gating mode (data not shown). These observations appear to rule out a role for phosphorylation, $PIP_2$, and polyamines in switching between Kv1.2 gating modes; however, further study is required to identify the interacting component that is responsible for the activation gating switch in Kv1.2 channels.

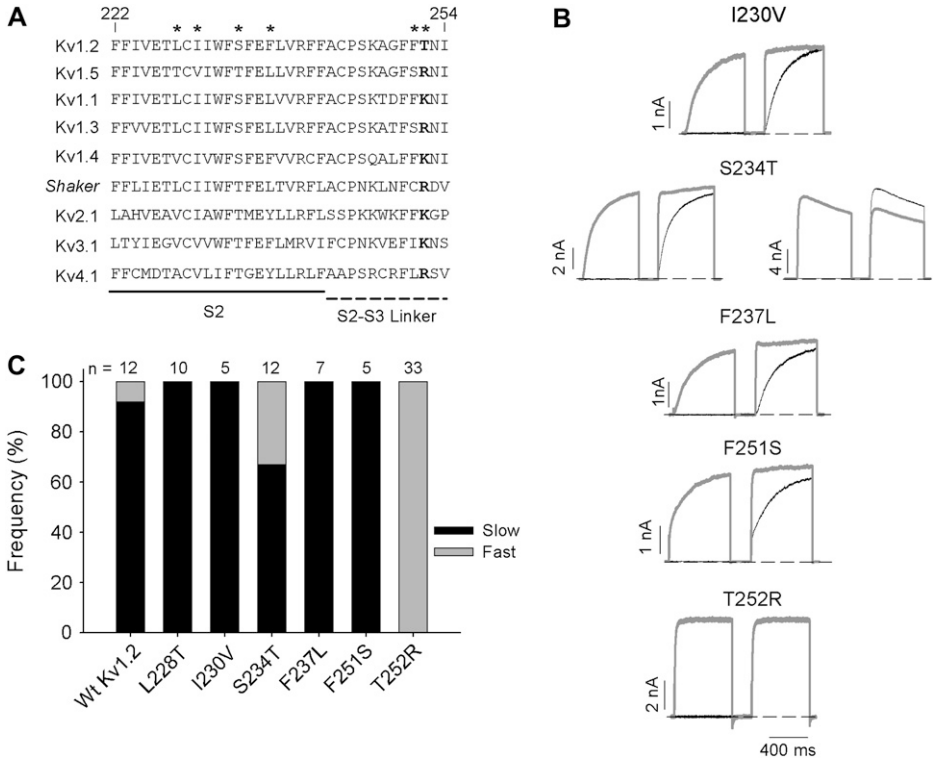


FIGURE 6 Point mutational study of the Kv1.2 S2 and S2-S3 linker. (*A*) Alignment of Kv1.2 and Kv1.5 S2 domains and S2-S3 linker with *Shaker* and other *Shaker*-related channels, Kv2.1, Kv3.1, and Kv4.1. Only six residues (marked above) are different between Kv1.2 and Kv1.5. All of these residues in Kv1.2 were mutated individually to the equivalent residues in Kv1.5, with the exception of L228T, which was covered in the Kv1.5S1S2L/Kv1.2 chimera (Fig. 4). (*B*) The activation properties of the constructs were studied using the twin-pulse protocol. Either a −50 mV or a +40 mV step was followed by a +40 mV test potential in the second step. Data with the +40 mV prepulse are shown in gray. The interpulse potential was −100 mV for 200 ms. (*C*) The frequency of ''slow'' and ''fast'' activation for each point mutation is shown as the proportion of solid and shaded in the bar graph, respectively. The recordings for Wt Kv1.2 and all the mutants were done on the same day with the exception of T252R, which was performed over a number of days. The number of cells studied for each construct is shown above.

## DISCUSSION

### ''Cell-to-cell'' versus ''pulse-to-pulse'' heterogeneity of Kv1.2 gating

This study has characterized a significant heterogeneity in the activation properties of heterologously expressed Kv1.2 channels. Our experiments demonstrate that Kv1.2 channels can exhibit at least two different gating phenotypes or modes in mammalian cells, which we have referred to as ''fast'' or ''slow''. Heterogeneity of the Kv1.2 current activation time course and voltage dependence between cells arises from differences in the proportion of channels occupying these two modes. Kv1.2 exhibits purely ''fast'' gating in a fraction of cells, purely ''slow'' gating in another fraction, and a mixture of the ''fast'' and ''slow'' modes in the remainder of cells (Fig. 1). The ''fast'' gating $V_{½}$ at ~−20 mV is reminiscent of reports of expression of Kv1.2 in oocytes ((28); −17.9 ± 0.5 mV) and, in the same preparation that we have used here, mouse fibroblasts (45).

Within individual cells exhibiting the ''slow'' gating phenotype, prepulse potentiation resulted in a predictable and reproducible acceleration of channel activation in a subsequent test pulse (Fig. 2), as first noticed by Grissmer et al. (46). Importantly, we could readily shift channels from the ''slow'' gating mode toward the ''fast'' gating mode, using depolarizing pulses above the threshold of current activation, and we were able to return channels from the ''fast'' gating mode and place them into the ''slow'' gating mode by holding cells for rest periods of 2 s or more at potentials of −40 mV and more negative (Fig. 3). Several lines of evidence suggest that the acceleration of activation during twin-pulse experiments is not caused by incomplete deactivation during the interpulse interval. Ionic current deactivation appeared complete with time constants of <20 ms at negative potentials (Fig. 3 *A*). Additionally, changing the holding potential over a wide range of voltages did not change the activation rate of channels exhibiting the ''slow'' phenotype, which suggests that ''slow'' and ''fast'' activation steps do not coexist in a single common activation pathway. In addition, recovery of the ''slow'' gating phenotype occurred most slowly at negative holding potentials, when channel deactivation would be expected to occur most rapidly (Fig. 3). Furthermore, conditioning channels with a depolarizing prepulse appeared to alter the voltage dependence of activation, resulting in an ~30 mV hyperpolarizing shift of the activation $V_{½}$ (Fig. 2 *E*). Collectively, these data suggest that prepulse potentiation of Kv1.2 reflects the existence of two pathways or modes of activation for this channel, with depolarization (sufficient for channel activation) favoring a shift of channels from the ''slow'' gating mode into the ''fast'' gating mode.

### A model scheme for ''fast'' and ''slow'' activation

A potential scheme describing the experimental data is shown in Fig. 9 (and see Materials and Methods). In the state diagram (Fig. 9 *A*), the upper row is similar to that modeled for *ShakerIR* when slow inactivation is excluded (26). Briefly, a voltage-dependent conformational change in each

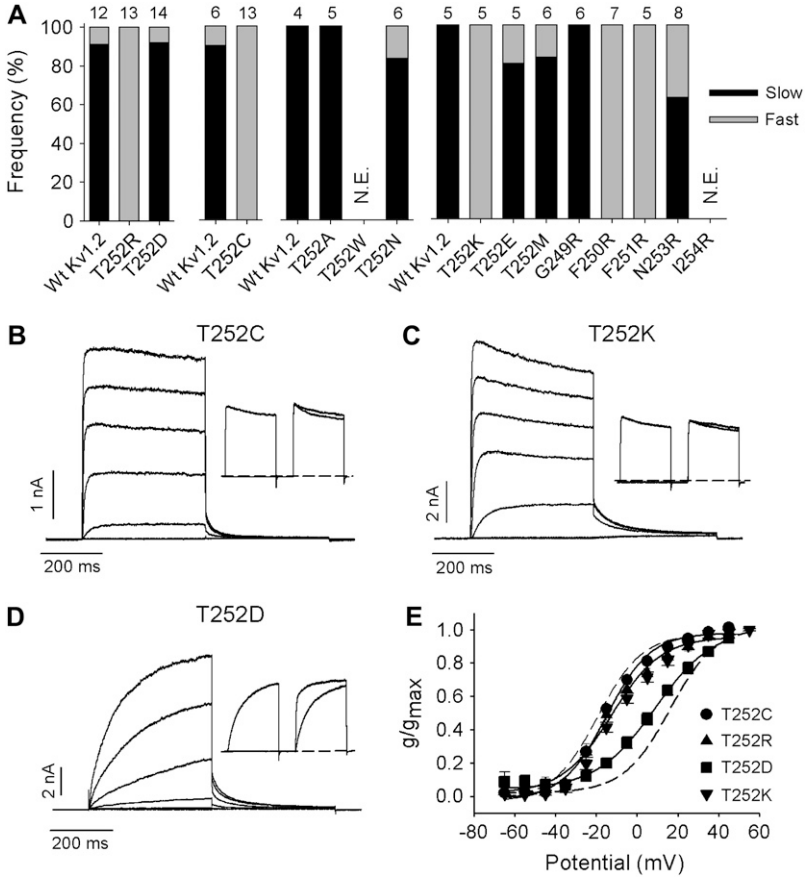


FIGURE 7 Activation effects of charged and uncharged substitutions of T252 in Kv1.2 and of residues in close proximity. (*A*) The activation properties of mutant constructs indicated on the abscissa were assessed using the twin-pulse protocol. Either a −50 mV or a +40 mV step was followed by a +40 mV test potential in the second step. The interpulse potential was −100 mV. N.E. = not expressed. The frequency of ''slow'' and ''fast'' activation for each point mutation is shown as the proportion of solid and shaded, respectively, in the bar graph. The number of cells studied for each construct is shown above. Wt Kv1.2 cells studied concurrently are shown in the leftmost bar for each data set. (*B–D*) Experimental examples of current-voltage data from constructs in *A*, T252C, T252K, and T252D. Currents were elicited by depolarizing steps from −65 to +55 mV in 20-mV increments. Insets illustrate the mutant response to the twin-pulse protocol described above for *A*. (*E*) The activation $V_{½}$ was −14 ± 1 mV ($n$ = 12, $k$ = 11.1 ± 0.6) for T252C (●), −11.2 ± 2.5 ($n$ = 6, $k$ = 14 ± 1.3) for T252R (▲), −10.3 ± 1.0 mV ($n$ = 4, $k$ = 13.7 ± 1.5) for T252K (▼) and +9.8 ± 2.3 mV ($n$ = 4, $k$ = 12.8 ± 0.8) for T252D (■). The broken curves illustrate the position of the mean isochronal conductance-voltage relations for ''fast'' and ''slow'' activating channels from Fig. 1 *E*.

of the four independent but identical subunits leads to a fully activated, not-open state ($C_4$), which can then undergo a concerted transition to the open state ($O_5$). As expected (26), slowing the rate of the concerted transition ($k_{co,s}$) in the lower gating tier so that it became the rate-limiting step and strongly biasing the vertical transitions to the ''slow'' activation pathway ($k_{fs} \gg k_{sf}$) produced currents with a predominantly slow activation time course that was well-fitted by a single exponential (not shown). However, constrained by the measured activation time constant-$V$ relation (Fig. 1 *G*), it was not possible, solely by slowing the concerted transitions ($C_{10} \rightarrow O_5$ and $C_{10} \leftarrow O_5$), to reproduce the depolarizing shift of the $g$-$V$ relation (Fig. 1 *E*). For that reason, in the final working version of the model to produce data in Figs. 9, *B–D*, an additional modification was made to the ''slow'' activation pathway to decrease the value for the microscopic activation rate constant $k_{f,s}$(0 mV). This modification, in turn, required the incorporation of the variable $d^x$, where x = 1–4, in the vertical transitions to conserve microscopic reversibility. Replication of currents showing only fast activation kinetics from a holding potential of −80 mV (Fig. 1 *C*) was achieved by altering the values for $k_{sf}$ and $k_{fs}$. The fast currents illustrated in Fig. 9 *B* were obtained by increasing $k_{sf}$ to 5 $s^{-1}$, which corresponds to a decrease of activation energy of 3.8 kcal/mol at 20°C.

The output of the model with the twin-pulse protocol is shown in Fig. 9 *E*. Both in the simulated and the experimental traces (Fig. 2 *A*), larger depolarizing prepulses increased the fast-activating current component. In the model this behavior arose because channels that reached $O_5$ along the ''slow'' pathway during the prepulse deactivated primarily along the upper gating tier, reaching $C_0$ and $C_1$ by the end the interpulse interval. Consequently, the larger the proportion of channels that reached $O_5$ during the prepulse, the larger the relative proportion of channels that activated via the ''fast'' pathway during the test pulse. Both the time dependence of the relaxation from the ''fast'' to the ''slow'' activation pathway in the two-pulse protocol (Fig. 3 *D*, $\tau \approx$ 4.5 s at −80 mV in the model), as well as a progressive enhancement of the peak current and fast-activating component with repeated 100-ms pulses to 10 mV at 2 Hz (seen experimentally, but not shown), were reproduced quite well by this gating scheme.

An interesting outcome of the twin-pulse voltage protocol is that after a strong depolarizing prepulse, the fast-activating test current at +20 mV showed a small, slow decay (Fig. 9 *E*). When a similar pattern was observed in experimental records (Fig. 2 *A*), it was provisionally attributed to coupling between activation and slow inactivation. However, the model, which explicitly excludes inactivation, indicated that

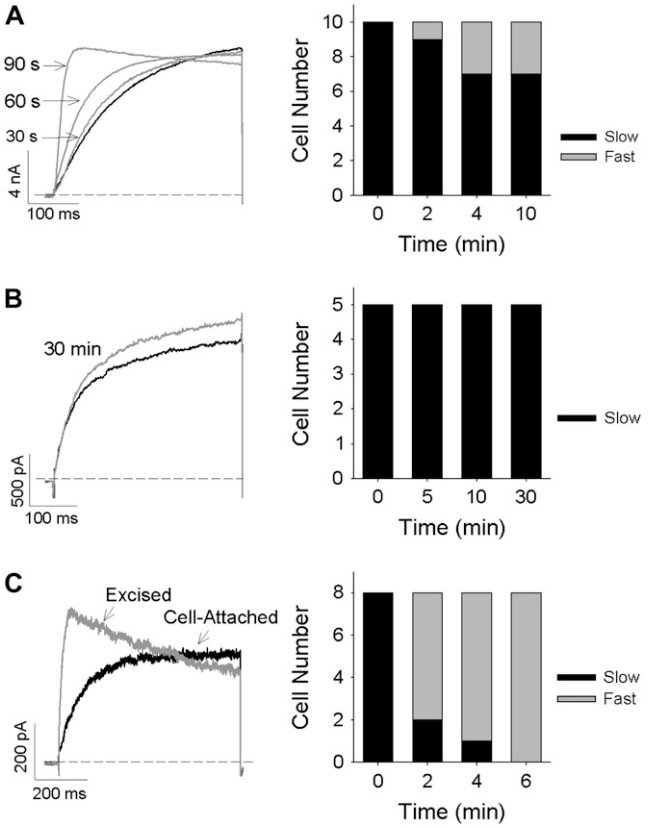


FIGURE 8 Kv1.2 channel gating can be modified by dialysis of cytosolic constituents. (*A* and *B*) Representative ionic currents (*left*) recorded in the whole-cell (*A*) and perforated-patch (*B*) configuration. Traces represent the current obtained immediately after breaking into the cell (*solid trace*; time = 0) and that recorded from the same cell 30 s, 60 s, and 90 s (in *A*) or 30 min (in *B*) later (*shaded traces*). Time dependence of the gating mode was seen in 3 of 10 cells in the whole-cell configuration but not in the perforated-patch configuration (*right bar graphs*). (*C*) Representative activating ionic currents (*left*) recorded from a cell-attached patch (*solid trace*) and after excision of the inside-out patch (*shaded trace*). An immediate switch from the ''slow'' to the ''fast'' gating mode was observed in eight of eight patches, which was complete 5 min after excision from the cell cytoplasm. In all cases ionic currents were recorded during depolarizing voltage steps to +40 mV at 30-s intervals from a holding potential of −80 mV.

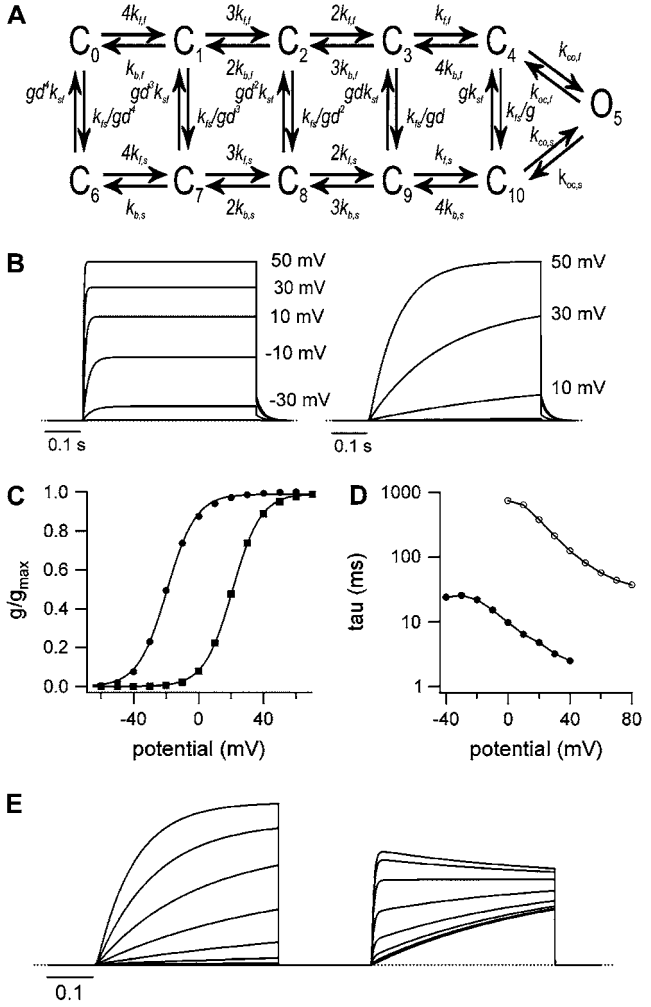


FIGURE 9 Model of ''fast'' and ''slow'' activation in Kv1.2. (*A*) Model gating scheme for Kv1.2. Two interconnected, parallel pathways representing ''fast'' (*upper*) and ''slow'' (*lower*) activation are connected to a single open state ($O_5$). Model kinetics are described in Methods. (*B*) To simulate the family of ''fast''-activating currents in the left panel, $k_{sf}$ was increased to 5 $s^{-1}$. Slowly activating currents are shown in the right panel. (*C*) Normalized *g-V* curves, derived from simulated currents and fitted to a Boltzmann function, gave $V_{½}$ of activation and *k* values, respectively, of −19.4 mV and +8.9 mV for the fast-activating currents (●) and +20.7 mV and +8.4 mV for ''slow''-activating currents (■). This approximates the nearly parallel, ~35 mV rightward shift of the *g-V* curve observed experimentally (Fig. 1 *E*). (*D*) For comparison to Fig. 1 *G*, the $\tau$-*V* relationship for the two families of currents was obtained as described in the Methods (i.e., exponential fit to the rising phase of the ''slow'' current; exponential fit from the half-amplitude time to the steady-state for fast, sigmoidal currents). (*E*) With a two-pulse voltage protocol, increasing the amplitude of the depolarizing prepulse from −10 to 50 mV increased the ''fast''-activating component of the test current evoked at 20 mV (compare with Fig. 2 *A*). The test current decay seen after a 50 mV prepulse is caused by a slow relaxation of channels from $C_4$ into the ''slow'' activation pathway ($C_7$–$C_{10}$).

a similar decay could arise from a slow transition of channels from $C_4$ into $C_{10}$ and subsequent redistribution into less-activated states ($C_7$–$C_9$). A prediction of the model is that this decay becomes less prominent at test voltages above +20 mV because both activation pathways are more strongly biased toward the open state (Fig. 10 *A*). Indeed, this is what is observed with this voltage protocol in experimental currents (Fig. 10 *B*) where inactivation is not an obvious confounding factor.

Although prepulse potentiation can transiently move channels into the ''fast'' gating mode, there is clearly a time-dependent recovery of ''slow'' gating (Fig. 3), with the balance of ''fast'' versus ''slow'' gating eventually returning to the level observed on break-in. This ''basal'' balance of ''fast'' versus ''slow'' channels is generally quite stable over durations required to complete the experiments reported here, although in several cells we were able to maintain a whole-cell recording for 30–40 min and observed a gradual

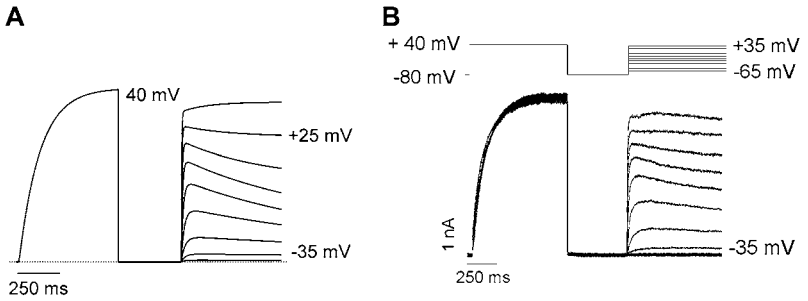


FIGURE 10 Simulated and experimental observation of dual activation pathways of Kv1.2 channel opening. (*A*) Traces were generated using the model of Kv1.2 gating (Fig. 9 *A*). A 600-ms pulse to +40 mV was followed by repolarization to −80 mV for 500 ms and then steps to potentials between −45 mV and +35 mV in 10-mV increments for 600 ms. The model predicts that after the +40 mV conditioning pulse, depolarization to potentials up to +25 mV (i.e., intermediate potentials) should give rise to current traces that activate rapidly and show a slow decay due to transitions from the late ''fast'' closed state ($C_4$) to the ''slow'' closed states ($C_7$-$C_{10}$), whereas depolarizing pulses to potentials >+25 mV should give rise to a fast activating current that is followed by a slow rising current, which is attributed to the opening of the channels that have made the transition from the late ''fast'' closed states to the ''slow'' gating state. (*B*) Experimental currents elicited by the voltage protocol shown above closely replicate the traces generated by the model.

disappearance of the ''slow'' gating phenotype (Fig. 8 *A*). This was prevented by performing experiments in the perforated patch clamp configuration (Fig. 8 *B*) and dramatically accelerated on excision of an inside-out patch (Fig. 8 *C*). The ''slow'' versus ''fast'' balance is therefore likely to be influenced by a cytoplasmic component that is uncontrolled in our experiments. On the basis of our model, we suggest that modification of the channel (phosphorylation, hydrogen bonding, or interaction with other proteins) can alter the values for transition rates between the ''slow'' and ''fast'' activation pathways and in doing so change the relative contributions of the two activation pathways to overall channel activation. Possible molecular mechanisms for this include variable expression of auxiliary subunits/binding partners or variable activation of one or more signaling pathways or other reversible posttranslational modification that could promote the ''slow'' gating mode of Kv1.2.

## Structural determinants of prepulse potentiation

Chimeric constructs of Kv1.2 and Kv1.5 allowed identification of the structural elements responsible for the ''slow'' gating behavior in Kv1.2 and its acceleration during twin pulses. Substitution of the S2-S3 linker of Kv1.2 with the sequence from the Kv1.5 channel completely abolished the ''slow'' gating phenotype, and we further delimited this effect to a single threonine (T252) in the Kv1.2 S2-S3 linker (Figs. 4–6). This segment of the protein is thought to be cytoplasmic (43), although its spatial relationship with other regions of the channel (either the cytoplasmic T1 domain or the transmembrane helices) remains uncertain. Only mutations at T252 or close by at F251 and F250 were able to abolish ''slow'' gating of Kv1.2 (Fig. 7 *A*). A possible explanation is that T252 and/or its immediate environment is directly involved in interactions that regulate the ''slow'' gating mode in Kv1.2, whereas mutations in other residues in the S2 segment can slightly alter the positioning/conformational arrangement of T252. Interestingly, substitution of the Kv1.2 S2 and S2-S3 linker into Kv1.5 imparted a ''slow'' gating phenotype in some cells (Fig. 5). However, the mutation Kv1.5 R356T (equivalent to Kv1.2 residue T252) did not confer ''slow'' gating. This suggests that other residues in the Kv1.2 S2 segment and S2-S3 linker may also be involved in regulating the ''slow'' gating behavior of this channel.

These data demonstrate that the S2 segment and S2-S3 linker are involved in the regulation of activation gating in Kv1.2 channels. Several studies that have demonstrated a critical role for the S2 segment in stabilizing positively charged residues in the S4 ''voltage sensor'' may be relevant to our findings (4,54). It has also been suggested that residues in the S2 transmembrane helix undergo rapid conformational changes early in the *Shaker* activation pathway (55). Whether this voltage-sensing role of S2 is involved in regulating the balance of channels occupying ''fast'' versus ''slow'' gating modes is unknown. However, it is worth mentioning again that the ''slow'' gating behavior (with essentially monoexponential activation kinetics, i.e., having little or no sigmoid character) of Kv1.2 appears to be governed by a rate-limiting transition very late in the activation pathway. Our most straightforward experimental support for this assertion is that slow activation kinetics in Kv1.2 persist even with very positive holding potentials just below the threshold for channel activation (Fig. 3). Thus, energetic effects on voltage-sensor movement at negative voltages do not provide an obvious explanation for the regulation of ''slow'' Kv1.2 gating by amino acids in the S2 segment or S2-S3 linker. Interestingly, although the S2-S3 linker was not resolved in the crystal structure of the Kv1.2 channel (43), the intracellular bases of the S2 and S3 helices, which constrain the S2-S3 linker, lie in close proximity to the S4-S5 linker region, which is thought to couple voltage sensor movement to opening of the activation gate (12). This suggests that the S2-S3 linker perhaps exerts its modulatory effect on the activation kinetics of the Kv1.2 channel by modifying late transitions that are coupled to opening of the pore.

Alignments within and across Kv channel subfamilies demonstrate that the homologous position to Kv1.2 T252 is almost universally occupied by a positively charged basic

residue (e.g., lysine or arginine). Introduction of lysine and arginine (T252R and T252K; Figs. 6 and 7) restored ''fast'' activation-gating properties that are evident in other Kv channels. The presence of threonine at 252 in Kv1.2 raises the interesting possibility that phosphorylation of this residue may play a role in regulation of ''slow'' gating. However, our attempts to mimic a phosphorylated state by the introduction of a fixed negative charge (T252D; Figs. 6 and 7) did not alter the heterogeneity of activation gating, given that the proportion of channels exhibiting ''slow'' activation kinetics was similar to Wt (Fig. 7). Additionally, the sequence in the region of T252 does not form a recognition sequence for any known protein kinase, and attempts with a broad-spectrum kinase inhibitor (e.g., staurosporine) or mixtures of specific Ser/Thr kinase inhibitors (Calbiochem, San Diego, CA) were unable to abolish the ''slow'' gating phenotype of Kv1.2 (data not shown). Another possible mechanism for regulation that cannot be ruled out is interaction with membrane phospholipids. In the Kir channel family, positively charged residues that lie near the membrane-fluid interface have been implicated in interactions with negatively charged headgroups of anionic phospholipids (e.g., $PIP_2$) in the inner leaflet of the plasma membrane, and these can dramatically alter channel gating by various ligands (56). However, application of $PIP_2$ to Kv1.2 inside-out patches did not alter activation gating properties (data not shown). Further studies are required to identify the cytoplasmic component that is involved with regulation of Kv1.2 activation gating.

Despite the lack of a role for phosphorylation and $PIP_2$ in the regulation of Kv1.2 activation properties, the observation that dialysis of the cell or separation of channels from the cytoplasmic constituents by forming excised patches causes a permanent switch of the activation gating from ''slow'' to ''fast'' (Fig. 8) suggests the involvement of a cytosolic component capable of modifying activation. In this study, we have been unable to identify the nature of this component, although we have ruled out phosphorylation by PKC, PKA, PKG, CaMKII and MLCK, and interaction of $PIP_2$ and polyamines (data not shown). The current data do, however, support the conclusion that activation gating in Kv1.2 can be regulated by interaction of a cytosolic gating modifier at or associated with T252 in the S2-S3 linker.

We thank Ms. Ka Kee Chiu for preparation of cells.

This work was supported by grants from the Heart and Stroke Foundation of British Columbia and Yukon, and the Canadian Institutes of Health Research (CIHR) to D.F. and S.J.K. S.R. was supported by graduate fellowships from the University of British Columbia and the Heart and Stroke Foundation of British Columbia and Yukon. H.T.K was funded by the Canadian Institutes of Health Research and the Michael Smith Foundation for Health Research. T.W.C. was supported by a postdoctoral research fellowship funded by a Focus on Stroke strategic initiative from The Canadian Stroke Network, the Heart and Stroke Foundation, the CIHR Institute of Circulatory and Respiratory Health, and the CIHR/Rx&D Program along with AstraZeneca Canada.

## REFERENCES

1. Seoh, S. A., D. Sigg, D. M. Papazian, and F. Bezanilla. 1996. Voltage-sensing residues in the S2 and S4 segments of the *Shaker* $K^+$ channel. *Neuron*. 16:1159–1167.
2. Papazian, D. M., L. C. Timpe, Y. N. Jan, and L. Y. Jan. 1991. Alteration of voltage-dependence of *Shaker* potassium channel by mutations in the S4 sequence. *Nature*. 349:305–310.
3. Liman, E. R., P. Hess, F. Weaver, and G. Koren. 1991. Voltage-sensing residues in the S4 region of a mammalian $K^+$ channel. *Nature*. 353:752–756.
4. Papazian, D. M., X. M. Shao, S. A. Seoh, A. F. Mock, Y. Huang, and D. H. Wainstock. 1995. Electrostatic interactions of S4 voltage sensor in *Shaker* $K^+$ channel. *Neuron*. 14:1293–1301.
5. Larsson, H. P., O. S. Baker, D. S. Dhillon, and E. Y. Isacoff. 1996. Transmembrane movement of the *Shaker* $K^+$ channel S4. *Neuron*. 16:387–397.
6. Bezanilla, F. 2000. The voltage sensor in voltage-dependent ion channels. *Physiol. Rev*. 80:555–592.
7. Aggarwal, S. K., and R. MacKinnon. 1996. Contribution of the S4 segment to gating charge in the *Shaker* $K^+$ channel. *Neuron*. 16: 1169–1177.
8. Del Camino, D., and G. Yellen. 2001. Tight steric closure at the intracellular activation gate of a voltage-gated $K^+$ channel. *Neuron*. 32: 649–656.
9. Elinder, F., R. Männikkö, and H. P. Larsson. 2001. S4 charges move close to residues in the pore domain during activation in a K channel. *J. Gen. Physiol*. 118:1–10.
10. Gandhi, C. S., E. Loots, and E. Y. Isacoff. 2000. Reconstructing voltage sensor-pore interaction from a fluorescence scan of a voltage-gated $K^+$ channel. *Neuron*. 27:585–595.
11. Ahern, C. A., and R. Horn. 2004. Stirring up controversy with a voltage sensor paddle. *Trends Neurosci*. 27:303–307.
12. Long, S. B., E. B. Campbell, and R. MacKinnon. 2005. Voltage sensor of Kv1.2: structural basis of electromechanical coupling. *Science*. 309: 903–908.
13. Glauner, K. S., L. M. Mannuzzu, C. S. Gandhi, and E. Y. Isacoff. 1999. Spectroscopic mapping of voltage sensor movement in the *Shaker* potassium channel. *Nature*. 402:813–817.
14. Cha, A., G. E. Snyder, P. R. Selvin, and F. Bezanilla. 1999. Atomic scale movement of the voltage-sensing region in a potassium channel measured via spectroscopy. *Nature*. 402:809–813.
15. Yellen, G. 2002. The voltage-gated potassium channels and their relatives. *Nature*. 419:35–42.
16. VanDongen, A. M. J., G. Frech, J. A. Drewe, R. H. Joho, and A. M. Brown. 1990. Alteration and restoration of $K^+$ channel function by deletions at the N- and C-termini. *Neuron*. 5:433–443.
17. Ju, M., L. Stevens, E. Leadbitter, and D. Wray. 2003. The Roles of N- and C-terminal determinants in the activation of the Kv2.1 potassium channel. *J. Biol. Chem*. 278:12769–12778.
18. Chiara, M. D., F. Monje, A. Castellano, and J. López-Barneo. 1999. A small domain in the N terminus of the regulatory $\alpha$-subunit Kv2.3 modulates Kv2.1 potassium channel gating. *J. Neurosci*. 19: 6865–6873.
19. Kurata, H. T., G. S. Soon, and D. Fedida. 2001. Altered state dependence of C-type inactivation in the long and short forms of human Kv1.5. *J. Gen. Physiol*. 118:315–332.
20. Kurata, H. T., G. S. Soon, J. R. Eldstrom, G. W. K. Lu, D. F. Steele, and D. Fedida. 2002. Amino-terminal determinants of U-type inactivation of voltage-gated $K^+$ channels. *J. Biol. Chem*. 277:29045–29053.
21. Aydar, E., and C. Palmer. 2001. Functional characterization of the C-terminus of the human *ether-à-go-go* related gene $K^+$ channel (HERG). *J. Physiol*. 534:1–14.
22. Wang, J. L., M. C. Trudeau, A. M. Zappia, and G. A. Robertson. 1998. Regulation of deactivation by an amino terminal domain in *human*

*ether-a-go-go-related gene* potassium channels. *J. Gen. Physiol.* 112: 637–647.

23. Minor, D. L., Jr., Y. F. Lin, B. C. Mobley, A. Avelar, Y. N. Jan, L. Y. Jan, and J. M. Berger. 2000. The polar T1 interface is linked to conformational changes that open the voltage-gated potassium channel. *Cell.* 102:657–670.
24. Cushman, S. J., M. H. Nanao, A. W. Jahng, D. DeRubeis, S. Choe, and P. J. Pfaffinger. 2000. Voltage dependent activation of potassium channels is coupled to T1 domain structure. *Nat. Struct. Biol.* 7:403–407.
25. Wang, G., and M. Covarrubias. 2006. Voltage-dependent gating rearrangements in the intracellular T1–T1 interface of a $K^+$ channel. *J. Gen. Physiol.* 127:391–400.
26. Smith-Maxwell, C. J., J. L. Ledwell, and R. W. Aldrich. 1998. Role of the S4 in cooperativity of voltage-dependent potassium channel activation. *J. Gen. Physiol.* 111:399–420.
27. Shieh, C. C., K. G. Klemic, and G. E. Kirsch. 1997. Role of transmembrane segment S5 on gating of voltage-dependent $K^+$ channels. *J. Gen. Physiol.* 109:767–778.
28. Koopmann, R., A. Scholle, J. Ludwig, T. Leicher, T. Zimmer, O. Pongs, and K. Benndorf. 2001. Role of the S2 and S3 segment in determining the activation kinetics in Kv2.1 channels. *J. Membr. Biol.* 182:49–59.
29. Uebele, V. N., S. K. England, A. Chaudhary, M. M. Tamkun, and D. J. Snyders. 1996. Functional differences in Kv1.5 currents expressed in mammalian cell lines are due to the presence of endogenous Kv$\beta$2.1 subunits. *J. Biol. Chem.* 271:2406–2412.
30. Accili, E. A., J. Kiehn, Q. Yang, Z. G. Wang, A. M. Brown, and B. A. Wible. 1997. Separable Kv$\beta$ subunit domains alter expression and gating of potassium channels. *J. Biol. Chem.* 272:25824–25831.
31. Heinemann, S. H., J. Rettig, H. R. Graack, and O. Pongs. 1996. Functional characterization of $K_v$ channel $\beta$-subunits from rat brain. *J. Physiol.* 493:625–633.
32. DeBiasi, M., Z. Wang, E. Accili, B. Wible, and D. Fedida. 1997. Open channel block of human heart hKv1.5 by the $\beta$-subunit hKv$\beta$1.2. *Am. J. Physiol.* 272:H2932–H2941.
33. McManus, O., L. M. H. Helms, L. Pallanck, B. Ganetsky, R. Swanson, and R. J. Leonard. 1995. Functional role of the $\beta$ subunit of high conductance calcium-activated potassium channels. *Neuron.* 14:645–650.
34. Perozo, E., and F. Bezanilla. 1990. Phosphorylation affects voltage gating of the delayed rectifier $K^+$ channel by electrostatic interactions. *Neuron.* 5:685–690.
35. Perozo, E., C. A. Vandenberg, D. S. Jong, and F. Bezanilla. 1991. Single channel studies of the phosphorylation of $K^+$ channels in the squid giant axon. I. Steady-state conditions. *J. Gen. Physiol.* 98:1–17.
36. Misonou, H., D. P. Mohapatra, E. W. Park, V. Leung, D. Zhen, K. Misonou, A. E. Anderson, and J. S. Trimmer. 2004. Regulation of ion channel localization and phosphorylation by neuronal activity. *Nat. Neurosci.* 7:711–718.
37. Mohapatra, D. P., and J. S. Trimmer. 2006. The Kv2.1 C terminus can autonomously transfer Kv2.1-like phosphorylation-dependent localization, voltage-dependent gating, and muscarinic modulation to diverse Kv channels. *J. Neurosci.* 26:685–695.
38. Macica, C. M., and L. K. Kaczmarek. 2001. Casein kinase 2 determines the voltage dependence of the Kv3.1 channel in auditory neurons and transfected cells. *J. Neurosci.* 21:1160–1168.
39. Thornhill, W. B., M. B. Wu, X. Q. Jiang, X. Y. Wu, P. T. Morgan, and J. F. Margiotta. 1996. Expression of Kv1.1 delayed rectifier potassium channels in Lec mutant Chinese hamster ovary cell lines reveals a role for sialidation in channel function. *J. Biol. Chem.* 271:19093–19098.
40. Watanabe, I., J. Zhu, J. J. Sutachan, A. Gottschalk, E. Recio-Pinto, and W. B. Thornhill. 2007. The glycosylation state of Kv1.2 potassium channels affects trafficking, gating, and simulated action potentials. *Brain Res.* 1144:1–18.
41. Watanabe, I., H. G. Wang, J. J. Sutachan, J. Zhu, E. Recio-Pinto, and W. B. Thornhill. 2003. Glycosylation affects rat Kv1.1 potassium channel gating by a combined surface potential and cooperative subunit interaction mechanism. *J. Physiol.* 550:51–66.
42. Ponce, A., E. V. S. De Miera, C. Kentros, H. Moreno, B. Thornhill, and B. Rudy. 1997. $K^+$ channel subunit isoforms with divergent carboxy-terminal sequences carry distinct membrane targeting signals. *J. Membr. Biol.* 159:149–159.
43. Long, S. B., E. B. Campbell, and R. MacKinnon. 2005. Crystal structure of a mammalian voltage-dependent *Shaker* family $K^+$ channel. *Science.* 309:897–903.
44. Steidl, J. V., and A. J. Yool. 1999. Differential sensitivity of voltage-gated potassium channels Kv1.5 and Kv1.2 to acidic pH and molecular identification of pH sensor. *Mol. Pharmacol.* 55:812–820.
45. Scholle, A., S. Dugarmaa, T. Zimmer, M. Leonhardt, R. Koopmann, B. Engeland, O. Pongs, and K. Benndorf. 2004. Rate-limiting reactions determining different activation kinetics of Kv1.2 and Kv2.1 channels. *J. Membr. Biol.* 198:103–112.
46. Grissmer, S., A. N. Nguyen, J. Aiyar, D. C. Hanson, R. J. Mather, G. A. Gutman, M. J. Karmilowicz, D. D. Auperin, and K. G. Chandy. 1994. Pharmacological characterization of five cloned voltage-gated $K^+$ channels, types Kv1.1, 1.2, 1.3, 1.5, and 3.1, stably expressed in mammalian cell lines. *Mol. Pharmacol.* 45:1227–1234.
47. Rezazadeh, S., H. T. Kurata, T. W. Claydon, S. J. Kehl, and D. Fedida. 2007. Modal gating of Kv1.2 channels mediated by the S2–S3 linker. *Biophys. J.* 92:467a (Abstr.).
48. Colquhoun, D., and A. G. Hawkes. 1995. A Q-matrix cookbook. *In* Single channel recording, 2nd ed. B. Sakmann and E. Neher, editors. Plenum Publishing Corp., New York. 589–633.
49. Hulme, J. T., E. A. Coppock, A. Felipe, J. R. Martens, and M. M. Tamkun. 1999. Oxygen sensitivity of cloned voltage-gated $K^+$ channels expressed in the pulmonary vasculature. *Circ. Res.* 85:489–497.
50. Fedida, D., B. Wible, Z. Wang, B. Fermini, F. Faust, S. Nattel, and A. M. Brown. 1993. Identity of a novel delayed rectifier current from human heart with a cloned $K^+$ channel current. *Circ. Res.* 73: 210–216.
51. Mohapatra, D. P., and J. S. Trimmer. 2006. The Kv2.1 C terminus can autonomously transfer Kv2.1-like phosphorylation-dependent localization, voltage-dependent gating, and muscarinic modulation to diverse Kv channels. *J. Neurosci.* 26:685–695.
52. Shyng, S. L., and C. G. Nichols. 1998. Membrane phospholipid control of nucleotide sensitivity of $K_{ATP}$ channels. *Science.* 282:1138–1141.
53. Oliver, D., C. C. Lien, M. Soom, T. Baukrowitz, P. Jonas, and B. Fakler. 2004. Functional conversion between A-type and delayed rectifier $K^+$ channels by membrane lipids. *Science.* 304:265–270.
54. Tiwari-Woodruff, S. K., C. T. Schulteis, A. F. Mock, and D. M. Papazian. 1997. Electrostatic interactions between transmembrane segments mediate folding of *Shaker* $K^+$ channel subunits. *Biophys. J.* 72: 1489–1500.
55. Cha, A., and F. Bezanilla. 1997. Characterizing voltage-dependent conformational changes in the *Shaker* $K^+$ channel with fluorescence. *Neuron.* 19:1127–1140.
56. Enkvetchakul, D., I. Jeliazkova, and C. G. Nichols. 2005. Direct modulation of Kir channel gating by membrane phosphatidylinositol 4,5-bisphosphate. *J. Biol. Chem.* 280:35785–35788.